

- Sciences, Washington, D.C. (1977).
25. For example, L. G. Hogan and D. S. Burch, *J. Chem. Phys.*, **65**, 894 (1976).
 26. For example, R. Gilpin, H. I. Schiff, and K. H. Welge, *ibid.*, **55**, 1087 (1971).
 27. M. Ogawa, *ibid.*, **53**, 3754 (1970).
 28. W. L. Wiese, M. W. Smith, and B. M. Miles, "Atomic Transition Probabilities," Natl. Stand. Ref. Data Ser. Nat. Bur. Stand. (U.S.), **4** (1966).
 29. R. M. Bedger, A. C. Wright, and R. F. Whitlock, *J. Chem. Phys.*, **43**, 4345 (1965).
 30. S. Banerjee, B. Shen, I. Chen, J. Bohlman, G. Brown, and R. Doering, *J. Appl. Phys.*, **65**, 1140 (1989).
 31. D. M. Smyth, G. A. Shirn, and T. B. Tripp, *This Journal*, **111**, 1331 (1964).
 32. H. Shinriki and M. Nakata, "Semiconductor World (in Japanese)," p. 113, Press Journal, Tokyo, May (1990).
 33. Y. Nishioka, S. Kimura, H. Shinriki, and K. Mukai, *This Journal*, **134**, 410 (1987).
 34. B. W. Shen, I.-C. Chen, S. Banerjee, G. A. Brown, J. Bohlman, P.-H. Chang, and R. R. Doering, "1987 IEEE IEDM Technical Digest," p. 582.
 35. R. S. Mulliken, *J. Chem. Phys.*, **3**, 573 (1935).
 36. F. A. Cotton and G. Wilkinson, Chap. 1 in "Basic Inorganic Chemistry," John Wiley & Sons, New York (1987).
 37. H. Tsubomura and M. Hori, *J. Syn. Org. Chem.*, **26**, 929 (1968).
 38. H. Okabe, in "Photo-chemistry of Small Molecules," John Wiley and Sons, Inc., New York (1978).

A Mathematical Model for Chemical Vapor Infiltration with Volume Heating

José I. Morell, Demetre J. Economou,* and Neal R. Amundson

Department of Chemical Engineering, University of Houston, Houston, Texas 77204-4792

ABSTRACT

A detailed mathematical model is presented to investigate the chemical vapor infiltration (CVI) of fiber-reinforced ceramic composites with a volume-heating source. Volume heating may be achieved by using microwave power or radio frequency (RF) induction in the case of conductive substrates. The analysis includes a set of constitutive equations describing the space and time dependence of species concentration, temperature, pressure, and porosity. The infiltration of carbon-fiber preforms with carbon resulting from methane decomposition is selected as a model system for analysis. Particular emphasis is placed on the impact of absorbed power on deposit uniformity and processing time. CVI with volume heating may lead to complete densification with considerably lower processing times when compared to conventional CVI processes. It is shown that when a constant power is used, there exists a critical power value above which accessible porosity is trapped within the composite. Several power modulation schedules are suggested to achieve rapid and complete densification without residual accessible porosity.

Advanced ceramics play a central role in satisfying the demands for materials with superior thermal, mechanical, electrical, and chemical properties needed in an increasing number of applications. Primary areas in which advanced ceramics may be utilized include heat-recovery systems, refractory products, tooling, combustors, separation systems, structural parts, aerospace components, and waste incineration systems (1). Fiber-reinforced ceramic composites have emerged as one of the most important materials to fulfill the aforementioned demands. Their main advantages are increased toughness, reliability, and wear resistance.

Among the techniques used for fabrication of fiber-reinforced ceramic composites (2, 3), chemical vapor infiltration (CVI) can meet important synthesis requirements such as low stress and processing temperatures. In addition, this technique can be used to synthesize solids with a fine-grain microstructure and to fabricate components of complex shape. In CVI, gaseous species infiltrate the interior of a preform and react to produce a solid material. There have been several types of CVI processes proposed during the years. They are generally classified as isothermal, thermal gradient, isothermal-forced flow, thermal gradient-forced flow, and pulsed flow. These processes vary mainly in the flow characteristics of the gaseous mixture and the heating scheme employed. However, the isothermal process is characterized by nonuniform deposition and long processing times that may reach several weeks. Some of the constraints associated with isothermal CVI have been overcome by using temperature and pressure gradients (4, 5). Nevertheless, the search for more efficient methods that yield rapid and complete densification continues. For a more extensive description of the different CVI processes the reader is referred to recent reviews by Lackey (6) and Besmann *et al.* (7) and the references therein.

Although there has been substantial progress in CVI in recent years, novel processes and synthesis techniques are still needed for the effective fabrication of ceramic composites. Mathematical models can provide insight into the physicochemical processes governing CVI as well as valuable guidelines for experimental research. The use of mathematical models can avoid time consuming and expensive trial and error practices and help in rapid evaluation of novel reactor designs and modes of operation.

Modeling studies of CVI have been increasing in number and complexity in the last several years. Starr (8) predicted changes in the composite structure of short-fiber preforms using a microstructural model. A pressure-driven, temperature-gradient CVI was studied by Tai and Chou (9) using a two-dimensional model for the deposition of SiC. A model for forced-flow CVI was recently proposed by Gupte and Tsamopoulos (10) in which equations for the conservation of mass, energy, and pore evolution were included. They concluded that forced-flow of reactants can improve uniformity of densification and found an optimum value of flow rate.

A better description of the pore structure evolution was incorporated by Melkote and Jensen (11) and Sotirchos and Tomadakis (12). In these studies, Monte Carlo simulations were used to model the dynamic changes of the structural parameters. Melkote and Jensen illustrated the dependence of porosity evolution on temperature when the preform was under isothermal and temperature-gradient conditions. Sotirchos and Tomadakis, on the other hand, investigated the effects of pressure pulsing on the uniformity of the infiltration process. Their analysis is among the few that has considered the full transient nature of CVI. Moreover, model results suggested that a better densification than that found experimentally may be possible by appropriate selection of operating parameters.

The use of microwave heating in the processing of ceramic materials has been recognized as a promising tech-

* Electrochemical Society Active Member.

nique. Microwave energy has been used for sintering, melting, calcining, drying, and joining (13). A distinct feature of microwave heating from the CVI point of view is that absorption of energy occurs throughout the volume of the composite (volume heating). This can lead to temperature profiles that favor the "inside-out" densification of the composite without residual accessible porosity. In the case of conductive substrates, radio frequency induction may be used to achieve volume heating. Indeed, Sugiyama and Ohzawa (14) observed "inside-out" densification of an inductively heated carbon preform infiltrated by SiC. Very recently, Gupta and Evans (15) reported a mathematical model of SiC CVI with microwave heating and external cooling. Apparently, this is the first study to consider the effect of volume heating on CVI. However, the authors used a very simplified model of the preform structure (a single-pore model) and did not consider the transient nature of the temperature of the composite as densification progresses.

This study is a comprehensive theoretical investigation of the physicochemical processes taking place in the chemical vapor infiltration of a cylindrical preform with volume heating. In particular, a carbon-fiber-reinforced carbon composite is selected to examine the general features of CVI with volume heating. The behavior of the system is described by a set of equations accounting for the dynamic changes in composition, temperature, pressure, and porosity. The model includes a comprehensive description of the multicomponent mass-transport processes and of the evolving pore structure. Particular emphasis is placed on the influence of absorbed power and time of exposure to a given power level on densification uniformity and total processing time. The results show that volume heating can lead to temperature profiles that favor the "inside-out" densification of the composite without residual accessible porosity. However, there exists a critical power above which otherwise accessible porosity is trapped within the composite. In such cases, a power modulation schedule can be used to obtain not only complete but also rapid densification.

Model Formulation

Conservation equations.—Mathematical modeling of CVI with volume heating involves the description of the transport and reaction phenomena occurring inside the composite. The system is characterized by the time evolution of species concentration, temperature, pressure, and pore structure. In general, important processes include the diffusion of gaseous species into and out of the fiber-matrix composite, the simultaneous occurrence of homogeneous and heterogeneous chemical reactions, and heat transfer due to conduction, convection, and radiation.

The system under consideration is a preform of cylindrical geometry with radius a in contact with a gas of known composition and temperature. The fibrous structure consists of cylindrical fibers randomly oriented in three-dimensional space. The statement of conservation of mass for gaseous species r is given by

$$\epsilon_A C \frac{\partial x_r}{\partial t} + \nabla \cdot J_r + N \cdot \nabla x_r = \sum_{i=1}^{n^R} \nu_{ri} R_i - x_r \sum_{r=1}^{n^G} \sum_{i=1}^{n^R} \nu_{ri} R_i \quad [1]$$

where ϵ_A is the accessible porosity, C is the total gaseous concentration, x_r is the mole fraction of the r th species, J_r and N are the diffusive and total molar flux, n^G and n^R are the number of gaseous species and chemical reactions considered in the model, and R_i is the rate per unit volume for the i th reaction. In order to investigate the effect of pressure variations inside the composite structure we state the following overall material balance

$$\frac{\partial(C\epsilon_A)}{\partial t} + \nabla \cdot N = \sum_{r=1}^{n^G} \sum_{i=1}^{n^R} \nu_{ri} R_i \quad [2]$$

The transport of individual species within the composite takes place by several mechanisms including molecular diffusion, Knudsen diffusion, and viscous flow. A comprehensive description of the transport processes ac-

counting for the above mechanisms can be obtained from the Dusty Gas model. This model provides expressions for the molar fluxes of each of the gaseous species as a function of mole fractions, diffusivities, transport parameters, and gradients in compositions and pressure. In terms of the molar flux of the r th species relative to the average molar velocity, J_r , and the total molar flux, N , the Dusty Gas model can be written as (16)

$$\sum_{s=1}^{n^G} \frac{x_s J_r - x_r J_s}{\Delta_{rs}} = - \frac{P}{RT} \nabla x_r - \frac{x_r}{RT} \left(1 - \frac{1}{D_r^e \sum_{s=1}^{n^G} x_s / D_s^e} \right) \nabla P = - A_r \quad [3]$$

$$N = - \frac{\sum_{s=1}^{n^G} J_s / D_s^e}{\sum_{s=1}^{n^G} x_s / D_s^e} - \frac{1}{RT} \left(\frac{B_0 P}{\eta} + \frac{1}{\sum_{s=1}^{n^G} x_s / D_s^e} \right) \nabla P \quad [4]$$

where Δ_{rs} is given by

$$\frac{1}{\Delta_{rs}} = \frac{1}{D_{rs}^e} + \frac{1}{D_r^e D_s^e \sum_{i=1}^{n^G} x_i / D_i^e} \quad [5]$$

Equations [3] and [4] along with the equation

$$\sum_{r=1}^{n^G} J_r = 0 \quad [6]$$

constitute a complete set of independent equations for the molar fluxes in a mixture of n^G species. For a three-component mixture, as the one considered in the present work (see below), solution of Eq. [3] and [6] provides the following explicit expressions for J_r

$$J_1 = - \Delta_{12} \Delta_{23} \Delta_{31} \frac{\{A_1 / \Delta_{23} - x_1 [A_1 (1 / \Delta_{23} - 1 / \Delta_{12}) + A_2 (1 / \Delta_{31} - 1 / \Delta_{12})]\}}{[x_1 (\Delta_{23} - \Delta_{12}) + x_2 (\Delta_{31} - \Delta_{12}) + \Delta_{12}]}$$

$$J_2 = - \Delta_{12} \Delta_{23} \Delta_{31} \frac{\{A_2 / \Delta_{31} - x_2 [A_1 (1 / \Delta_{23} - 1 / \Delta_{12}) + A_2 (1 / \Delta_{31} - 1 / \Delta_{12})]\}}{[x_1 (\Delta_{23} - \Delta_{12}) + x_2 (\Delta_{31} - \Delta_{12}) + \Delta_{12}]}$$

The energy balance is given by the following expression

$$C_p^e \frac{\partial T}{\partial t} - \nabla \cdot (k^e \nabla T) + \sum_{r=1}^{n^G} (N_r C_{p,r}) \cdot \nabla T + \sum_{i=1}^{n^R} (\Delta H_i R_i) = (1 - \epsilon) \Phi \quad [9]$$

where C_p^e and k^e are the effective thermal capacity per unit volume and effective thermal conductivity of the fiber-matrix composite, respectively, and ϵ is the total porosity. The first term on the left side of Eq. [9] is an accumulation term, whereas the second to fourth terms account for conduction, convection, and heat of reaction, respectively. The term on the right side represents the power absorbed by the fiber-matrix composite. It is assumed that power is absorbed by the solid phase only and that the power absorbed per unit volume of solid, Φ , is constant. Φ may be time dependent, however, and this can be used to optimize the CVI process as shown later. Cases of position dependent Φ will be examined in later studies.

Table I. Dimensionless variables and parameters.

Symbol	Definition
A_r^*	$A_r/(a/C)^{ref}$
f_{2s}	D_s^e/D^{ref}
f_3	k^e/k^{ref}
β_i	$(-\Delta H_i^0)/(CD/(Tk))^{ref}$
β^*	B_o/B^{ref}
γ	$\bar{\epsilon}\sigma(aT^0/k)^{ref}$
Δ_{rs}^*	Δ_{rs}/D^{ref}
ζ	r/a^{ref}
η^*	η/η^{ref}
θ	T/T^{ref}
λ	$\alpha^{ref}N/(CD)^{ref}$
λ_r	$\alpha^{ref}N_r/(CD)^{ref}$
Λ_i	$R_i\alpha^{ref2}/(CD)^{ref}$
Le	$C_p^e D^{ref}/k^{ref}$
Le_{gr}	$C_{gr}^e (CD/k)^{ref}$
Le_{sk}	$C_{sk}^e (CD/k)^{ref}$
μ_r	$\alpha^{ref}J_r/(CD)^{ref}$
Nu	$h(a/k)^{ref}$
$\bar{\Xi}_c$	$M_c C^{ref}/\rho_c$
Π	P/P^{ref}
τ	$t(D/a^2)^{ref}$
Φ^*	$\Phi(a^2/Tk)^{ref}$
ψ	$(B_o/P/\eta D)^{ref}$

The evolution of accessible porosity as well as its dependence on position can be obtained from the following equation

$$\frac{\partial \epsilon_A}{\partial t} = - \frac{M_c}{\rho_c} \sum_{i=1}^{nR} \nu_{ci} R_i \quad [10]$$

in which M_c and ρ_c are the molecular weight and density of the deposited carbon, respectively. The rate of i th reaction per unit volume of composite, R_i , can be expressed as

$$R_i = \begin{cases} \epsilon_A R_i^* & \text{for a homogeneous reaction rate} \\ S_A R_{si} & \text{for a heterogeneous reaction rate} \end{cases}$$

where R_i^* is the reaction rate per unit volume of gas (see for example Eq. [35]), R_{si} is the reaction rate per unit surface area, and S_A is the accessible surface area per unit volume of composite. The latter can be obtained from the literature (17, 18).

The governing equations are subject to the following boundary and initial conditions

$$\text{BC1-3: at } r = 0 \quad \nabla x_r = 0, \nabla P = 0, \nabla T = 0 \quad [11]$$

BC4-6: at $r = a$

$$x_r = x_{rb}, P = P_b, -k^e \nabla T = h(T - T_b) + \sigma \bar{\epsilon} (T^4 - T_b^4) \quad [12]$$

$$\text{IC1-4: at } t = 0 \quad x_r = x_{ro}, P = P_o, T = T_o, \epsilon_A = \epsilon_{A,o} \quad [13]$$

BC1-3 stipulate that at the center of the preform there is no flux of any of the gaseous species or flux of energy. At the edge of the preform we have set the composition of the gaseous species as well as the pressure to be constant, as indicated by BC4 and BC5. BC6 implies that the preform loses heat by convection and radiation to an environment of constant temperature T_b .

The modeling equations and the corresponding boundary and initial conditions can be restated in dimensionless form, with the introduction of the dimensionless variables listed in Table I, as follows

$$0 < \zeta < \zeta^*$$

$$\Pi \frac{\epsilon_A}{\theta} \frac{\partial x_r}{\partial \tau} + \frac{1}{\zeta} \frac{\partial}{\partial \zeta} (\zeta \mu_r) + \frac{\partial x_r}{\partial \zeta} \lambda = \sum_{i=1}^{nR} \nu_{ri} \Lambda_i - x_r \sum_{r=1}^{nG} \sum_{i=1}^{nR} \nu_{ri} \Lambda_i \quad [14]$$

$$\frac{\partial}{\partial \tau} \left(\epsilon_A \frac{\Pi}{\theta} \right) + \frac{1}{\zeta} \frac{\partial}{\partial \zeta} (\zeta \lambda) = \sum_{r=1}^{nG} \sum_{i=1}^{nR} \nu_{ri} \Lambda_i \quad [15]$$

$$\mu_1 = -\Delta_{12}^* \Delta_{23}^* \Delta_{31}^*$$

$$\frac{\{A_1^*/\Delta_{23}^* - x_1[A_1^*(1/\Delta_{23}^* - 1/\Delta_{12}^*) + A_2^*(1/\Delta_{31}^* - 1/\Delta_{12}^*)]\}}{[x_1(\Delta_{23}^* - \Delta_{12}^*) + x_2(\Delta_{31}^* - \Delta_{12}^*) + \Delta_{12}^*]} \quad [16]$$

$$\mu_2 = -\Delta_{12}^* \Delta_{23}^* \Delta_{31}^*$$

$$\frac{\{A_2^*/\Delta_{31}^* - x_2[A_1^*(1/\Delta_{23}^* - 1/\Delta_{12}^*) + A_2^*(1/\Delta_{31}^* - 1/\Delta_{12}^*)]\}}{[x_1(\Delta_{23}^* - \Delta_{12}^*) + x_2(\Delta_{31}^* - \Delta_{12}^*) + \Delta_{12}^*]} \quad [17]$$

$$\lambda = - \frac{\sum_{s=1}^{nG} \mu_s M_s^{1/2}}{\sum_{s=1}^{nG} x_s M_s^{1/2}} - \frac{1}{\theta} \left(\frac{\psi \Pi \beta^*}{\eta^*} + \frac{1}{\sum_{s=1}^{nG} x_s / f_{2s}} \right) \frac{\partial \Pi}{\partial \zeta} \quad [18]$$

$$\begin{aligned} Le \frac{\partial \theta}{\partial \tau} - \frac{1}{\zeta} \frac{\partial}{\partial \zeta} \left(\zeta f_3 \frac{\partial \theta}{\partial \zeta} \right) + \sum_{r=1}^{nG} Le_{gr} \lambda_r \frac{\partial \theta}{\partial \zeta} &= \sum_{i=1}^{nR} \beta_i \Lambda_i \\ &+ (1 - \epsilon) \Phi^* - \sum_{r=1}^{nG} \sum_{i=1}^{nR} \nu_{ri} \Lambda_i \int_{\theta_0}^{\theta} Le_{gr} d\theta \\ &- \sum_{k=1}^{nS} \sum_{i=1}^{nR} \nu_{ki} \Lambda_i \int_{\theta_0}^{\theta} Le_{sk} d\theta \quad [19] \end{aligned}$$

$$\frac{\partial \epsilon_A}{\partial \tau} = - \bar{\Xi}_c \sum_{i=1}^{nR} \nu_{ci} \Lambda_i \quad [20]$$

Boundary and initial conditions

$$\text{BC1-3: at } \zeta = 0 \quad \nabla x_r = 0, \nabla \Pi = 0, \nabla \theta = 0 \quad [21]$$

BC4-6: at $\zeta = \zeta^*$

$$x_r = x_{rb}, \Pi = \Pi_b, -f_3 \nabla \theta = Nu(\theta - \theta_b) + \gamma(\theta^4 - \theta_b^4) \quad [22]$$

$$\text{IC1-4: at } \tau = 0 \quad x_r = x_{ro}, \Pi = \Pi_o, \theta = \theta_o, \epsilon_A = \epsilon_{A,o} \quad [23]$$

Preform structure and model parameters.—In order to provide a comprehensive description of the CVI process it is necessary to incorporate into the formulation of the mathematical model a realistic representation of the fiber architecture and its time evolution. Such a description should provide the dependence of the structural parameters and species diffusivities on the morphology of the composite. In the present study, the cylindrical preform is envisioned as consisting of identical cylindrical fibers randomly positioned in three-dimensional space. Recently, Melkote and Jensen (17) and Tomadakis and Sotirchos (18) have modeled the aforementioned fiber structure as a population of overlapping cylinders using a Monte Carlo technique. They determined the effective Knudsen diffusion coefficients as well as the surface area, permeability coefficient, and accessible porosity as a function of total porosity. Based on these studies, one can obtain useful relations for the description of the solid structure without formally preforming extensive numerical computations. In particular, Fig. 1 shows the variation of the accessible porosity as a function of total porosity used in the present work. This figure illustrates the formation of inaccessible porosity as the porosity decreases, and the existence of a percolation threshold at a porosity level of 10%.

The formulation of the mathematical model incorporates several parameters which characterize the composite structure as well as transport properties of the diffusing multicomponent mixture. These parameters depend, in general, on temperature, pressure, and composition of the gaseous mixture. The effective binary diffusion coefficient, D_{rs}^e , and Knudsen diffusion coefficient, D_s^e , are obtained from the following relations

$$D_{rs}^e = \epsilon_A \epsilon D_{rs} \quad [24]$$

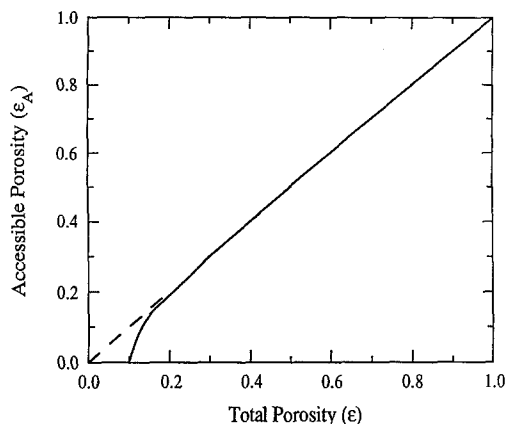


Fig. 1. Dependence of accessible porosity on total porosity.

$$D_s^e = w(\epsilon)D_s \quad [25]$$

where the polynomial, $w(\epsilon)$, was used to fit results obtained by Melkote and Jensen (17) for Knudsen diffusion in a three-dimensional section of randomly placed fibers. The binary diffusion coefficients D_{rs} are estimated from (19)

$$D_{rs} = 1.858 \times 10^{-7} \frac{\sqrt{T^3(1/M_r + 1/M_s)}}{P\sigma_{rs}^2\Omega_{rs}} \quad [26]$$

in which σ_{rs} is a mean collision diameter and Ω_{rs} is the collision integral. The Knudsen diffusion coefficient is defined by

$$D_s = \frac{2}{3} \bar{r}_p \sqrt{\frac{8RT}{M_s\pi}} \quad [27a]$$

with

$$\bar{r}_p = -\frac{r_f}{\ln \epsilon} \quad [27b]$$

where \bar{r}_p is the average pore radius. The effective value of the permeability factor is obtained from the relation

$$B_o = \frac{\bar{r}_p^2}{8} \epsilon_A \epsilon \quad [28]$$

The viscosity of the gaseous species as a function of temperature is estimated from (19)

$$\eta_r = 2.6693 \times 10^{-5} \frac{\sqrt{M_r T}}{\sigma_r^2 \Omega_{\mu r}} \quad [29]$$

in which σ_r is the collision diameter and $\Omega_{\mu r}$ is a collision integral dependent on temperature and on the characteristic energy of interaction between molecules. The thermal conductivity and effective heat capacity of the preform are given by the following expressions

$$k^e = (1 - \epsilon)^2 k_s + \epsilon^2 k_G \quad [30]$$

$$C_p^e = (1 - \epsilon) \sum_{k=1}^{nS} c_k^s C_{pk}^s + \epsilon \sum_{r=1}^{nG} c_r C_{pr} \quad [31]$$

The dependence of the i th heat of reaction on temperature is given by

$$\Delta H_i = \Delta H_i^0 + \sum_{s=1}^n \nu_{is} \int_{T_0}^T C_{ps} dT \quad [32]$$

The variation of the heat capacity with temperature can be expressed in a polynomial form as

$$C_{ps} = a_s + b_s T + c_s T^2 + d_s T^3 \quad [33]$$

where the constants a_s , b_s , c_s , and d_s are tabulated in several sources [e.g., Ref. (20) and (21)].

Chemical kinetics.—The deposition of carbon by the decomposition of methane is taken as a model chemical system in the present work. The mechanism and kinetics of the thermal decomposition of methane have been the subject of many studies. The importance of methane decomposition partially lies on applications associated with the CVI of carbon-carbon composites (4), and the deposition of diamond films (e.g., 22, 23). Despite the fact that the gas-phase chemistry is relatively well understood, knowledge of surface processes is still very incomplete.

Experimental investigations conducted by Palmer and Hirt (24), Skinner and Ruehrwein (25), and Kevorkian *et al.* (26) have shown that the decomposition reaction is first-order in methane concentration. These studies suggest that the process is limited by the initial rupture of the C-H bond. The present work focuses on the effect of novel methods for heating the preform to optimize product density and processing time. Hence, simplified chemical kinetics are used whereby the deposition of carbon is described by an overall reaction as shown by the following equation



In this simplified scheme, the carbon deposition rate equals the methane decomposition rate given by

$$R_1^* = C_{\text{CH}_4} k_1 \exp[-E_1/(RT)] \quad [35]$$

The pre-exponential factor and activation energy were taken as $k_1 = 2.24 \times 10^{14}$ 1/s and $E_1 = 3.64 \times 10^5$ J/mol, respectively, close to the values reported by Kevorkian *et al.* (26). In accordance with Eq. [34], three gaseous components are included in the model, namely, methane, hydrogen, and argon (an inert).

Method of solution.—The model equations subject to the associated boundary and initial conditions were solved by the method of lines. The numerical solution can be simplified substantially by substituting the explicit flux relations (Eq. [7] and [8]) in the mass-balance equations [1]. This procedure reduces the set of equations obtained after spatial discretization solely to a system of differential equations (instead of a differential-algebraic equation system). The technique of orthogonal collocation on finite elements with B-splines basis functions (27) was employed for the discretization of the spatial derivatives. Following this method, the piecewise polynomial approximation of each of the dependent variables can be written, in terms of the B-splines basis functions, as follows

$$u_m(\tau, \zeta) = \sum_{j=1}^{n^c} c_{j,m}(\tau) B_j(\zeta) \quad [36]$$

where u_m represents the m th dependent variable, the set $\{B_j; j = 1, \dots, n^c\}$ consists of the B-splines basis functions, and $c_{j,m}$ are unknown coefficients dependent only on time, while the known basis functions B_j depend only on position, ζ . Substitution of Eq. [36] into the partial differential equations and associated boundary conditions while requiring its validity at a set of n^c collocation points reduces the model to a system of ordinary differential equations. The resulting set of differential equations was integrated in the time variable using a variable-step, variable-formula method (28). The simulations reported in this study involved approximately 400 unknowns and were performed on a CRAY-YMP supercomputer. The CPU time needed to obtain the solution varied from 0.2 to 5 minutes depending on the parameter values used.

Results and Discussion

The following results provide insight into the nature of the transport and reaction processes affecting CVI with volume heating, and the dependence of these phenomena on the parameters employed. We will examine how the level of heating power influences the deposition uniformity and time of densification. The physical properties of the preform, kinetic parameters, and reference conditions used in the calculations are given in Table II. To elucidate the trends in system behavior and to have a basis for com-

Table II. System parameters and reference conditions.

$k_1 = 2.24 \times 10^{14}$ m/s		$E_1 = 3.64 \times 10^5$ J/mol
$\Delta H_1^\circ = 7.484 \times 10^4$ J/mol		
$D_1^e = 12.11 w(\epsilon) d_p T^{0.5}$, m ² /s	$D_2^e = 34.16 w(\epsilon) d_p T^{0.5}$, m ² /s	
$D_3^e = 7.67 w(\epsilon) d_p T^{0.5}$, m ² /s	$D_{12} = 1.224 \times 10^{-8} T^{1.5} / (P\Omega_{12})$, m ² /s	
$D_{13} = 4.192 \times 10^{-9} T^{1.5} / (P\Omega_{13})$, m ² /s	$D_{23} = 1.337 \times 10^{-8} T^{1.5} / (P\Omega_{23})$, m ² /s	
$M_1 = 16.04$ g/mol	$M_2 = 2.016$ g/mol	
$M_3 = 39.944$ g/mol	$\rho_c = 1.74$ g/cm ³	
$\alpha^{\text{ref}} = 1.0$ mm	$B^{\text{ref}} = 1.25 \times 10^{-13}$ m ²	
$D^{\text{ref}} = 1.25 \times 10^{-4}$ m ² /s	$k^{\text{ref}} = 6.58 \times 10^{-2}$ J/(m s K)	
$T^{\text{ref}} = 1000$ K	$P^{\text{ref}} = 1$ atm	
$k_G = 4.516 \times 10^{-3} T^{0.5}$ J/(m s K)	$k_s^{-1} = 0.239 (2.4 + 3.46 \times 10^{-3} T)$ (m s K)/J	

parison, the base values of all parameters shown in Table III are used first. These values are employed unchanged throughout the simulations unless otherwise stated. In the following paragraphs, accessible porosity refers to the volume fraction of the composite which is available for mass transport and hence belongs to the set of conduits that act as passages for reactants and products. Trapped accessible porosity refers to that volume fraction which is trapped in the composite as a result of, for example, surface pore closure. This porosity would otherwise be accessible for mass transport.

In order to compare theoretical predictions with experimental data, we first consider that infiltration takes place at constant temperature and pressure. The description of the isothermal-isobaric system is provided by the set of equations given above excluding the energy balance and neglecting the viscous flux contribution to the molar fluxes. The densification data used for comparison are those reported by Devlin *et al.* (29) for the pyrolytic deposition of carbon on fiber bundles. The values for pressure, species mole fraction, temperature, and initial porosity were selected to be identical to those given by Devlin *et al.* (29). Figure 2 presents model predictions (solid lines) and experimental data (points) in terms of the mass gain as a function of time for several values of temperature. Trends forecast by the model are in good agreement with the experimental data. At low temperatures, the evolution of mass gain is characterized by an almost linear dependence on time. As temperature increases, however, the mass gain dependence on time turns into sublinear at later times. Although the trends are captured by the model, the densification is over-predicted at high and low temperatures, whereas the reverse is true at intermediate temperatures. This may be due to the very simplified reaction mechanism used. The incorporation of a detailed mechanism accounting for both homogeneous and heterogeneous reactions may be necessary for a more realistic description of the process.

The present work pertains to a preform structure which can be modeled by a population of overlapping cylinders. This structural model is quite different from the fiber bundle used by Devlin *et al.* (29). However, because the experimental data of Devlin *et al.* were taken under kinetically controlled conditions, and since a homogeneous reaction was used here to describe the deposition rate, the only structural parameter entering the model is the accessible porosity (see Eq. [10]) and not the details of the preform structure. Calculations using a one-dimensional preform structure to simulate the fiber bundle used by Devlin *et al.* gave results identical to those of Fig. 2. It was therefore felt

Table III. Basic parameter values used for calculations.

Symbol	Name	Basic value
a	Preform radius	1 mm
$\epsilon_{A,0}$	Initial accessible porosity	0.5
Nu	Nusselt number	0.2
P_0	Initial pressure	1 atm
r_f	Fiber radius	4.0 μ m
T_b	Ambient temperature	300 K
x_{1b}	Methane mole fraction	0.6
x_{2b}	Argon mole fraction	0.4

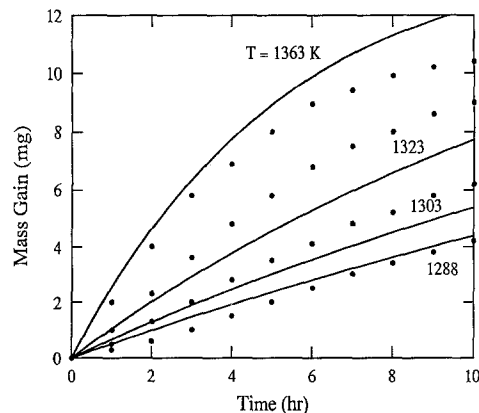


Fig. 2. Variation of mass gain with time for isothermal CVI of carbon-carbon composites. Points are data of Devlin *et al.* Solid lines are model predictions.

that comparison of the model predictions with the data of Devlin *et al.* could still be performed to test the appropriateness of using the first-order homogeneous kinetics (Eq. [35]) to describe the deposition rate. Of course, when species transport in the preform and/or heterogeneous reactions are important, the preform structure is essential for describing the system behavior.

CVI under isothermal conditions at a temperature of 1400 K was found to be kinetically controlled, resulting in nearly uniform porosity and concentration profiles inside the preform. Although excellent deposit uniformity is obtained in the kinetically controlled regime, the associated processing times are long. The use of a higher temperature may reduce the processing time only to compromise the uniformity of the deposition process since diffusion limitations become more important as the temperature increases. This characteristic is illustrated in Fig. 3a which shows the radial variation of the accessible porosity with time at a temperature of 1700 K. One can clearly see the development of steep porosity gradients in the vicinity of the composite surface as well as the eventual sealing of the surface pores and the entrapment of porosity within. For the same operating conditions, Fig. 3b shows the depletion of methane and its inability to diffuse into the composite as densification occurs from "outside-in." Therefore, the process is limited by diffusion of the reactant inside the composite. It is also observed that a large concentration of hydrogen is built up within the composite as CVI progresses.

We now investigate the behavior of CVI with volume heating using the parameter values of Table III. The results that follow are shown in terms of the dimensionless power Φ^* (see Table I). The variation of accessible porosity with position and time is shown in Fig. 4a for a dimensionless power of 7.14. For the parameter values used, this would correspond to a power density of 4.7×10^8 W/m³. One observes the development of a reaction zone starting from the center of the composite and moving towards the surface. This "inside-out" densification pattern is a consequence of the temperature distribution in the composite. Since the composite is heated uniformly and loses heat to its surroundings by radiation and convection, the center temperature is highest as depicted in Fig. 4b. This temperature profile slows down the reaction near the preform surface, allowing for penetration of reactant deep into the composite. As infiltration proceeds, increasingly more carbon is deposited, and the porosity approaches and subsequently attains the percolation limit first in the composite center. This results in steeper porosity gradients at later times, testifying to the interplay between temperature and concentration profiles and their effect on the deposition process. Eventually, the densification is complete without early surface closure resulting in a fiber-matrix composite with excellent density uniformity.

Figure 5 shows the evolution of porosity profiles for a dimensionless power of 9.12 (6.0×10^8 W/m³). The corresponding temperature profiles are similar to those of

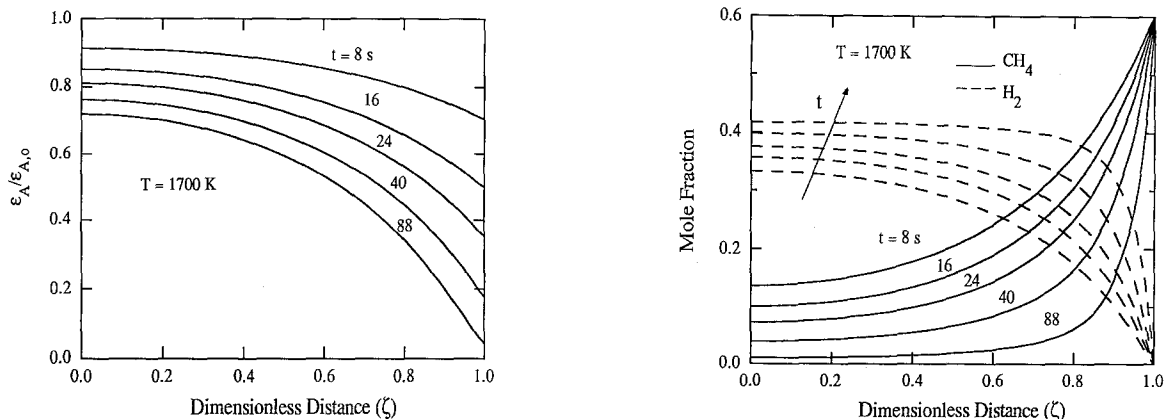


Fig. 3. (a, left) Evolution of accessible porosity profiles for isothermal CVI at 1700 K. (b, right) Evolution of species concentration profiles for the same conditions given in (a).

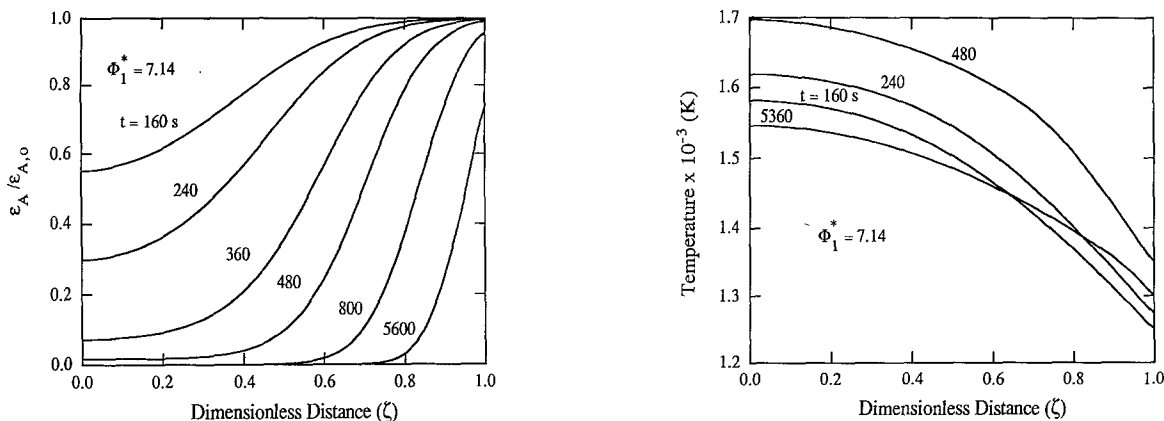


Fig. 4. (a, left) Evolution of accessible porosity profiles for CVI with volume heating using a dimensionless power of $\Phi_1^* = 7.14$. (b, right) Evolution of temperature profiles for the same conditions given in (a).

Fig. 4b except that the temperatures are higher for the higher value of Φ^* . For these higher temperatures the reaction rate is rapid enough to cause significant reactant depletion as methane diffuses into the composite. Therefore, deposition deeper in the composite is limited by reactant supply despite the fact that the temperature is higher there. This in turn causes the formation of a minimum in the porosity profile which at a time of 112 s is located at a dimensionless distance of about 0.5. As densification progresses, the porosity keeps on decreasing close to the surface, further hindering the transport of species deep into the preform. The final result is entrapment of otherwise accessible porosity within the preform. One also notices that beyond a densification time of 352 s the deposition process becomes much slower as demonstrated by the times corre-

sponding to the last two profiles. These results suggest that the power level employed has a strong effect on densification. Therefore, power control may be used to optimize the CVI process.

The discussion up to this point has focused on the effect of power on the uniformity of the deposit. To explore the effect of power on processing time, we have defined $\tau_{10\%}$ as the time required for the average accessible porosity to reach 10% of its initial value. The variation of the processing time, $\tau_{10\%}$, as a function of power is illustrated in Fig. 6. It is observed that the processing time initially decreases with an increase in power, reaches a minimum, and then increases with further increase in power. This behavior can be explained in terms of physicochemical processes governing CVI. At low power levels the densification is kinetically controlled, and the processing times are long. As

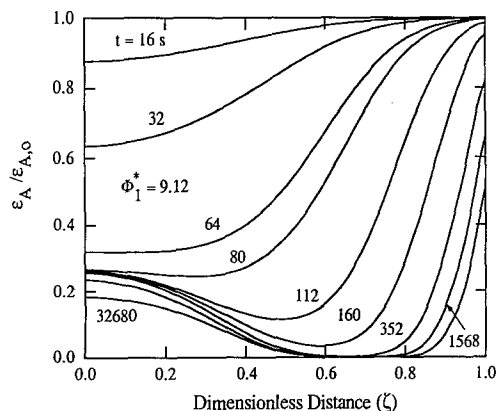


Fig. 5. Evolution of accessible porosity profiles for CVI with volume heating using a dimensionless power of $\Phi_1^* = 9.12$.

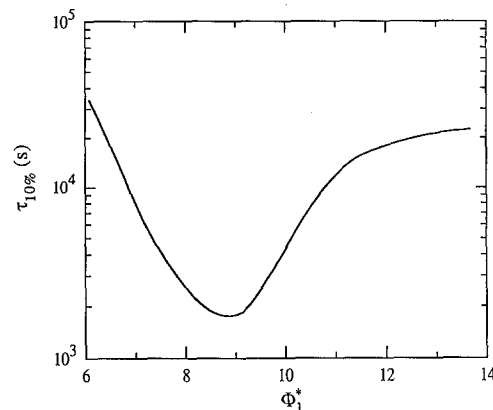


Fig. 6. Dependence of processing time on power.

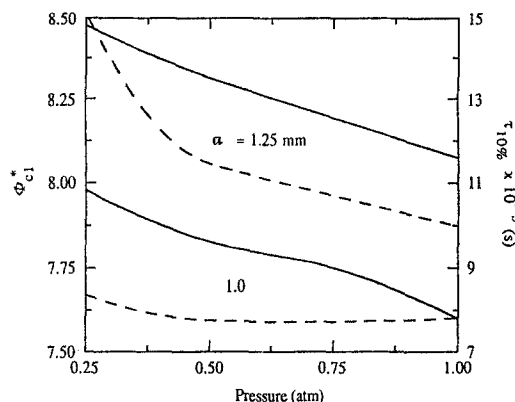


Fig. 7. Dependence of the critical value of power and processing time on pressure for two values of preform radius.

power, and hence temperature, increases the deposition rate increases resulting in lower processing times. Beyond a dimensionless power of about 9.0, however, progressively higher temperatures attained by the composite lead to reactant depletion and hence long times to fill the inner zones of the preform (see also Fig. 5). For even higher values of Φ^* , the process is controlled totally by diffusion, and the processing times are almost independent of power (i.e., independent of temperature). Despite the existence of an optimum value of power that gives minimum processing time, uniformity considerations may preclude the use of such a value.

The critical power Φ_{cl}^* was defined as the value of power above which a minimum develops in the porosity profile. Continued deposition beyond this minimum would result in porosity which is otherwise accessible to be trapped within the composite (see for example Fig. 5). For a given system, one would prefer to operate at power levels below the critical to achieve complete densification. Figure 7 presents the critical power, Φ_{cl}^* , as a function of reactor pressure (solid lines). The processing time when the power is set at 90% of Φ_{cl}^* is also shown (dashed lines). Because lower pressures lead to higher diffusivities and therefore higher mass-transport rates, it is found that a decrease in pressure is followed by a corresponding increase in Φ_{cl}^* . This suggests that deposit nonuniformities may be partially alleviated by using lower pressure, although this may also result in a larger $\tau_{10\%}$. Results for a preform with radius $a = 1.25$ mm (the base value is 1 mm) show the same qualitative trends. Although the nondimensional value of the critical power is higher for higher a the value of the actual critical power is lower (remember that Φ_{cl}^* varies as a^2). This is because an increase in preform radius results in larger diffusional resistance, which requires lower values of Φ_{cl} to avoid premature pore plugging. Examination of the processing times corresponding to a preform radius of 1 mm reveals that they are almost independent of pressure down to a value of about 0.3 atm. These represent the lowest processing times one could obtain, while avoiding the development of any residual accessible porosity. For $a = 1.25$ mm, $\tau_{10\%}$ increases faster with decreasing pressure due to lower temperatures prevailing inside the preform.

The previous analysis has revealed that deposit uniformity may be one of the most important criteria in determining the value of power, and that this value can have a dramatic effect on processing time. In pursuit of new approaches that result in complete densification while minimizing the processing time, we now study the impact of a variable power heating source. In particular, we will consider a scheduling in which the power is initially set at a value higher than Φ_{cl}^* for a certain period of time, and then is decreased to a value lower than Φ_{cl}^* until completion of the densification process. The dependence of power on time is thus described by a step function. Results for this power scheduling are shown in Fig. 8. $\Phi_{1,80}^* = 9.12$ implies that a power of 9.12 units is used first (subscript 1) for 80 s. Beyond that time a power of $\Phi_2^* = 7.0$ units is used. The switching is done just before the occurrence of a mini-

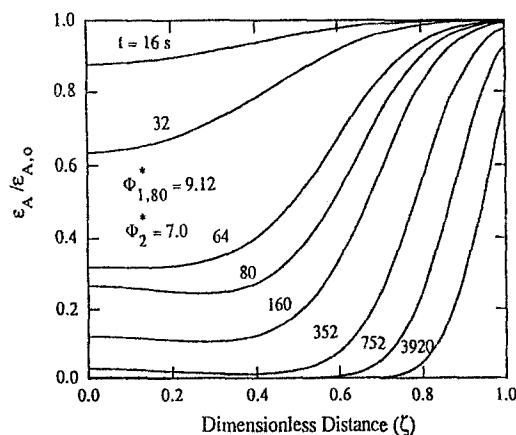


Fig. 8. Evolution of accessible porosity profiles with a step function power modulation. A dimensionless power of 9.12 was used for the first 80 s followed by a power of 7.0.

imum in the porosity profiles. When compared to Fig. 5, for which the power was kept constant at 9.12, Fig. 8 reveals that power scheduling has a significant effect on the way the porosity profiles unfold. Due to the lower temperatures in the composite after a time of 80 s, there is deeper infiltration of methane into the composite. As a result, pore plugging is completely avoided.

The choice of Φ_2^* in the previous simulation was partially arbitrary. The only stipulation was that Φ_2^* be lower than the critical value (which is 7.60 for the conditions of Fig. 8; see also Fig. 7). Since power has a substantial effect on processing time, it is useful to determine the critical value of Φ_2^* beyond which residual accessible porosity develops. Results are shown in Fig. 9 which should be read as follows: for a given value of Φ_1^* , deposition is carried out to a point that a minimum in the porosity profile is incipient. At that time the power should be switched to Φ_{c2}^* shown in Fig. 9. Any power higher than Φ_{c2}^* would result in residual accessible porosity. Any power lower than Φ_{c2}^* would result in an unnecessarily longer processing time. The cumulative processing time for the optimum process is shown in Fig. 9. It can be seen that the curve of Φ_{c2}^* vs. Φ_1^* possesses a minimum at about $\Phi_1^* = 9.2$, where $\tau_{10\%}$ possesses a maximum at about the same location. There are two competing factors responsible for such behavior, namely, composite temperature and switching time. As Φ_1^* increases, the temperature takes on higher values, and therefore Φ_{c2}^* has to decrease to avoid reactant depletion. At the same time, however, the switching time decreases since a higher Φ_1^* leads to an earlier development of a dip in the porosity profiles. This results in the formation of a minimum in Φ_{c2}^* and a maximum in $\tau_{10\%}$ at an intermediate value of initial power Φ_1^* .

Another approach to optimize the process is to use power scheduling with two changes of power level. First, a high power is used until the porosity at the composite center attains the percolation limit. Then the power is

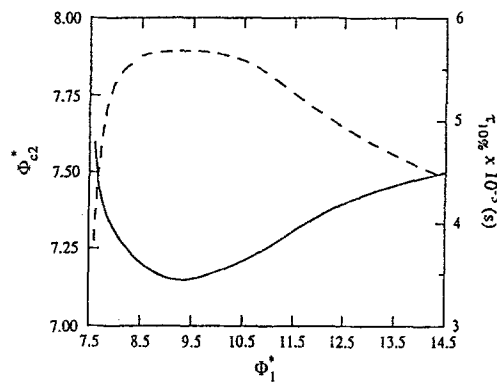


Fig. 9. Dependence of critical power after switching Φ_{c2}^* , and total processing time on power before switching, Φ_1^* .

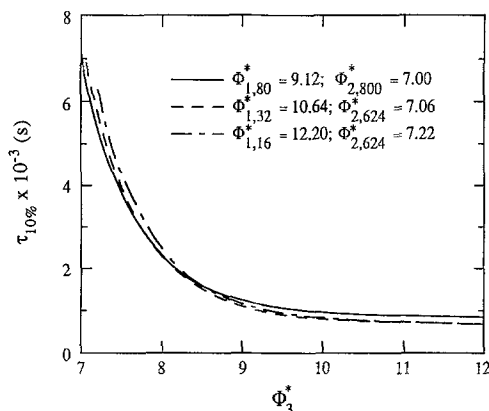


Fig. 10. Dependence of processing time on Φ_3^* for several power schedules. For example, the solid line corresponds to starting with a dimensionless power of 9.12, switching to power 7.00 at 80 s, then switching again to Φ_3^* at 800 s.

switched to a lower value to "fill" most of the composite except for a zone around the periphery. Finally, the power is switched again to a high level to densify the composite completely. This scheme can provide rapid and complete densification. The processing time with this power scheduling is shown in Fig. 10 for three cases. In all these cases complete densification was achieved without any trapped accessible porosity. The solid line corresponds to values of Φ_1^* and Φ_2^* used in Fig. 8. In the present case a power of 9.12 is used first. At 80 s the power is switched to a value of 7.0 and at 800 s the power is switched again to Φ_3^* . It is seen that $\tau_{10\%}$ decreases dramatically as Φ_3^* is increased. However, beyond a value of about 9.0 the processing time becomes almost independent of Φ_3^* as the system enters the diffusion-controlled regime. It is also observed that all three cases behave almost identically, which suggests that Φ_3^* may be chosen independently of previous choices of power level, as long as qualitatively the same porosity evolution is obtained.

The previous analysis indicates that, when following a step function power modulation schedule, the power level(s) and switching time(s) must be carefully selected in order to obtain "optimum" results. We realize that in practice this selection may require considerable experimentation and experience with a particular CVI process. The above examples illustrate that the mathematical model can provide valuable guidelines in optimizing the power scheduling.

Pressure gradient effects.—The importance of a self-generated pressure gradient on the densification process was also explored. Pressure variation effects are incorporated into the mass-transport equations as an additive contribution to each of the diffusive molar fluxes (see Eq. [3]). This contribution depends on the pressure gradient as well as the permeability of the preform and the viscosity of the gaseous mixture. The existence of pressure variations within the composite (despite the fact that a constant pressure is maintained outside) may be due to an increase or decrease in the number of moles because of reaction. Consequently, it is conceivable that pressure variations may affect the behavior of the system. It was found, however, that self-generated pressure gradients had a negligible effect on the densification process throughout the parameter range explored in this study. Interestingly enough, the pressure was found to be lower inside the composite although the methane decomposition reaction leads to an increase in the number of moles. Nevertheless the pressure variations were very small (less than 3%). The decrease in pressure within the preform was a consequence of the replacement of methane molecules by hydrogen molecules as deposition took place. Since hydrogen has the lowest molecular weight in the system, it can diffuse more rapidly out of the composite, effectively increasing the outward molar flux, resulting in a lower pressure inside the composite.

Summary and Conclusions

A detailed mathematical model has been developed for the chemical vapor infiltration of fiber-reinforced ceramic composites with a volume-heating source. Volume heating may be achieved by using microwave power or radio frequency induction in the case of conductive substrates. The fabrication of a carbon-carbon composite using methane as a carbon source was examined. The mathematical formulation consisted of a set of partial differential equations describing the physicochemical processes occurring inside the preform, when exposed to a multicomponent gas mixture. The mass transport of gaseous species in the evolving solid structure was described using an explicit form of the Dusty Gas model with variable physical properties. The numerical solution of the governing equations, using the technique of orthogonal collocation on finite elements provided the space and time dependence of composition, temperature, pressure, and porosity in a wide region of the parameter space.

Simulations emphasized the impact of power and time of exposure at a given power level on deposit uniformity and processing time. The evolution of accessible porosity, temperature, and species concentration was determined under isothermal and volume heating conditions. For the isothermal system, model predictions compared fairly well with available experimental data. For the case of volume heating, the influence of power, pressure, preform size, and viscous flow on the dynamics of the process was examined. Several power modulation schemes were suggested to optimize the densification process.

Volume heating resulted in favorable temperature profiles in the composite which, depending on the power level, yielded an "inside-out" deposition and therefore complete densification. For a constant applied power, a critical value of power, Φ_{ci}^* , existed above which residual accessible porosity was trapped within the composite. The processing time exhibits a minimum as a function of power, but this minimum may be above Φ_{ci}^* , i.e., it may result in trapped porosity. Dramatic improvements in uniformity with minimum processing time were obtained by using several step-function power-modulation schemes. Simulation results showed that judicious selection of the power levels and switching times can result in rapid and complete densification without any residual accessible porosity.

The dynamic changes in pressure caused by the development of viscous flow were found to be minimal in all the simulations performed. Nevertheless, it was revealed that the pressure actually decreases inside the composite even though there is an increase in the number of moles during deposition. The replacement of a heavier gas (methane) by a lighter one (hydrogen) was responsible for this behavior.

The mathematical formulation presented here accounts for important phenomena such as the transient nature of the process, the evolution of the preform structure, heat transfer, and multicomponent mass transfer. However, there are uncertainties associated with the evaluation of the effective transport properties. Furthermore, greatly simplified reaction kinetics were used, since the purpose was to examine alternate heating schedules that may improve the product density and lower the processing time. Finally, the effect of heating schedules on composite microstructure and mechanical properties of the final product was not addressed. Therefore, the results should be seen as a set of guidelines for predicting the system behavior and for optimizing the CVI process.

Acknowledgments

The authors are grateful to the Pittsburgh Supercomputer Center for making computer time available on the CRAY-YMP supercomputer.

Manuscript submitted May 8, 1991; revised manuscript received Sept. 4, 1991.

The University of Houston assisted in meeting the publication costs of this article.

LIST OF SYMBOLS

a	preform radius, m
A_r	defined by Eq. [3]
B_o	permeability, m^2
B_j ($j = 1, \dots, n^c$)	B-spline basis function
$C_{j,m}$	unknown coefficients, see Eq. [36]
C	gas mixture concentration, $kmol/m^3$
C_k^s	concentration of the k th solid species, kg/m^3
C_{pr}	heat capacity of the r th gaseous species, $kJ/(kmol K)$
C_{pk}^{ss}	heat capacity of the k th solid species, $kJ/(kg K)$
C_p^e	effective heat capacity of the composite, $kJ/(m^3 K)$
D_r	Knudsen diffusion coefficient, m^2/s
D_{rs}	binary diffusion coefficient of the r - s pair, m^2/s
E_i	activation energy of the i th reaction, $kJ/kmol$
f_{2s}	dimensionless Knudsen diffusion coefficient
f_3	dimensionless effective thermal conductivity
h	heat transfer coefficient, $J/(m^2 s K)$
J_r	molar flux of the r th species relative to the molar average velocity, $kmol/(m^2 s)$
k_G, k_s, k^e	thermal conductivity of the gas mixture, of the solid, and of the composite, respectively, $kJ/(m s K)$
Le	effective Lewis number
Le_{gr}	Lewis number of the r th gaseous species
Le_{sk}	Lewis numbers of the k th solid species
M_r	molecular weight of the r th species, $kg/kmol$
N, N_r	total molar flux and molar flux of the r th species, respectively, $kmol/(m^2 s)$
Nu	Nusselt number
n^G, n^R, n^S	number of gaseous species, reactions, and solid species, respectively
P	pressure, atm
r	radius coordinate, m
r_p	average porous radius, m
R	gas constant, $m^3 atm/(kmol K)$
R_i	rate of the i th reaction per unit volume of composite, $kmol/(m^3 s)$
R_i^*	rate of the i th reaction per unit volume of gas, $kmol/(m^3 s)$
t	time, s
T	temperature, K
x_r	mole fraction of the r th species
Greek	
β_i	dimensionless heat of the i th reaction
β^*	dimensionless permeability factor
γ	dimensionless group, Table I
ΔH_i	heat of the i th reaction, $kJ/kmol$
Δ_{rs}	defined by Eq. [5], m^2/s
ϵ, ϵ_A	total porosity and accessible porosity, respectively
$\bar{\epsilon}$	emissivity of carbon
ζ	dimensionless distance
η	viscosity of the gaseous mixture, $kg/(m s)$
θ	dimensionless temperature
λ, λ_r	dimensionless total molar flux and flux of the r th species, respectively
Λ_i	dimensionless reaction rate
μ_r	dimensionless molar flux relative to the molar-average velocity
ν_{ri}	stoichiometric coefficient for species r in reaction i
Ξ_c	dimensionless group, Table I
Π	dimensionless pressure
ρ_c	density of deposited carbon, kg/m^3
σ	Stefan-Boltzmann constant, $J/(m^2 s K^4)$
σ_{rs}	mean collision diameter, m
τ	dimensionless time
$\tau_{10\%}$	processing time, s
Φ	power of volume-heating source, W/m^3
Ω_{rs}	collision integral
ψ	dimensionless group, Table I

Subscripts

o	initial value
b	bulk or ambient value
r ($r = 1, 2, 3$)	CH_4, H_2 and Ar , respectively
c	carbon

Superscripts

o	values computed at temperatures T^o
ref	value computed at the reference conditions
e	effective value
*	dimensionless value

REFERENCES

1. M. A. Karnitz, D. F. Craig, and S. L. Richlen, *Am. Ceram. Soc. Bull.*, **70**, 430 (1991).
2. J. A. Cornie, Y-M. Chiang, D. R. Uhlmann, A. Mortensen, and J. M. Collins, *ibid.*, **65**, 293 (1986).
3. J. R. Strife, J. J. Brennan, and K. M. Prewo, *Ceram. Eng. Sci. Proc.*, **11**, 871 (1990).
4. W. V. Kotlensky, *Chem. Phys. Carbon*, **9**, 173 (1973).
5. A. J. Caputo and W. J. Lackey, *Ceram. Eng. Sci. Proc.*, **5**, 654 (1984).
6. W. J. Lackey, *ibid.*, **10**, 577 (1989).
7. T. M. Besmann, R. A. Lowden, B. W. Sheldon, and D. P. Stinton, in "Chemical Vapor Deposition 1990," K. E. Spear and G. W. Cullen, Editors, PV 90-12, p. 482, The Electrochemical Society Softbound Proceedings Series, Pennington, NJ (1990).
8. T. L. Starr, *Ceram. Eng. Sci. Proc.*, **8**, 951 (1987).
9. N-H Tai and T-W Chou, *J. Am. Ceram. Soc.*, **73**, 1489 (1990).
10. S. M. Gupte and J. A. Tsamopoulos, *This Journal*, **137**, 3675 (1990).
11. R. R. Melkote and K. F. Jensen, in "Chemical Vapor Deposition of Refractory Metals and Ceramics," T. M. Besmann and B. M. Gallois, Editors, p. 67, Materials Research Society, Pittsburgh, PA (1990).
12. S. V. Sotirchos and M. M. Tomadakis, in *ibid.*, p. 73.
13. W. H. Sutton, *Am. Ceram. Soc. Bull.*, **68**, 376 (1989).
14. K. Sugiyama and Y. Ohzawa, *J. Mater. Sci.*, **25**, 4511 (1990).
15. D. Gupta and J. W. Evans, *J. Mater. Res.*, **6**, 810 (1991).
16. R. Jackson, "Transport in Porous Catalysts," Elsevier Pub. Co., New York (1977).
17. R. R. Melkote and K. F. Jensen, *AICHE J.*, **35**, 1942 (1989).
18. M. M. Tomadakis and S. V. Sotirchos, *ibid.*, **37**, 74 (1991).
19. R. B. Bird, W. E. Stewart, and E. N. Lightfoot, "Transport Phenomena," John Wiley & Sons, Inc., New York (1960).
20. D. M. Himmelblau, "Basic Principles and Calculations in Chemical Engineering," 4th ed., Prentice-Hall, Englewood Cliffs, NJ (1982).
21. R. H. Perry and C. H. Chilton, "Chemical Engineers' Handbook," 5th ed., McGraw Hill, Inc., New York (1973).
22. M. Frenklach, *J. Appl. Phys.*, **65**, 5142 (1989).
23. S. J. Harris, *ibid.*, **65**, 3044 (1989).
24. H. B. Palmer and T. J. Hirt, *J. Phys. Chem.*, **67**, 709 (1963).
25. G. B. Skinner and R. A. Ruehrwein, *J. Phys. Chem.*, **63**, 1736 (1959).
26. V. Kevorkian, C. E. Heath, and M. Boudart, *ibid.*, **64**, 964 (1960).
27. C. de Boor, "A Practical Guide to Splines," Springer-Verlag, New York (1978).
28. L. Petzold, *SIAM J. Stat. Comput.*, **4**, 136 (1983).
29. D. J. Devlin, R. S. Barbero, and R. P. Currier, in "Chemical Vapor Deposition 1990," K. E. Spear and G. W. Cullen, Editors, PV 90-12, p. 499, The Electrochemical Society Softbound Proceedings Series, Pennington, NJ (1990).